Time resolved coherent anti-Stokes Raman scattering of I_2 isolated in matrix argon: Vibrational dynamics on the ground electronic state

M. Karavitis, R. Zadoyan, and V. Ara Apkarian[a)]
Department of Chemistry, University of California, Irvine, California 92697-2025

(Received 16 August 2000; accepted 14 December 2000)

Time-resolved, electronically resonant, coherent anti-Stokes Raman scattering is used to prepare and interrogate vibronic coherences of molecular iodine in matrix Ar. Coherences that involve evolution on the excited $B(^3\Pi_{0u})$ state, first- and third-order coherences, decay in less than one vibrational period ($\tau<300$ fs). In contrast, as many as 200 vibrational periods of motion can be observed for Raman-prepared wave packets consisting of zero-phonon vibrational superpositions on the ground electronic state (second-order coherence). Packets consisting of $v=4$, 5 and $v=3$, 4, 5 on the $X(^1\Sigma_g)$ state decay with a half-life of 10 ± 1 ps at 31 K, allowing a more accurate measure of vibrational level spacings and decoherence time than has been possible in frequency domain. The harmonic frequency of the molecule is reduced by 1.5 cm^{-1} (0.7%) in the matrix. The lack of recurrence in the excited electronic state ensures that the resonant anti-Stokes scattering arises only from the negative momentum component of the Raman packet. This momentum filter, which should be ubiquitous in condensed media, leads to a signal with deeper modulation than in the gas phase.
 [DOI: 10.1063/1.1346643]

I. INTRODUCTION

We report the first time-resolved four-wave mixing measurements in rare gas matrices, in the form of coherent anti-Stokes Raman scattering (CARS) of I_2 isolated in matrix Ar. The experiment combines the elements of preparation, manipulation, and interrogation of vibronic coherences in this condensed phase prototype. To date, time resolved measurements of matrix isolated iodine have been limited to pump–probe studies of population dynamics on excited electronic states.[1,2] CARS interrogates coherences in which the electronic phase is preserved in the four-wave interaction.[3] Moreover, CARS gives access to vibrational coherences on the ground electronic surface, about which the existing information is convoluted in line shapes of frequency domain resonant Raman (RR) spectra.[4] Indeed, as coherent spectroscopy, the information content in CARS is in principle obtainable through frequency domain measurements. There are, however, both practical and fundamental considerations in the choice of the measurement domain. In the present example, it will be possible to obtain information at a higher resolution than has been practical in frequency domain RR measurements.[5,6] More fundamental is the consideration that time-resolved CARS (TRCARS) allows a three-pulse manipulation of wavepackets, an aspect unique to the time-domain, and the main motivation behind our studies. In this context, with regard to coherence control,[7] this model system remains useful for developing strategies in condensed media.[8–13]

The principles of CARS, in both time and frequency domain, are well established, and the method has been applied extensively in all media.[3,14,15] With the accessibility of ultrafast laser sources, there has been significant development in real-time TRCARS studies. The very diverse aims pursued in this field may be illustrated with examples of applications in liquid phase dynamics,[16] studies of biomolecules *in vivo* and *in vitro*,[17] to carrier dynamics in solids,[18] band dynamics in superlattices,[19] to the interrogation of molecular solids,[20] to microscopy.[21] Most intimately related to the present are the recent series of fs CARS investigations in iodine vapor.[22] There, due to the thermal population of rotational states, it is the molecular rovibronic coherence that is prepared and interrogated. A complete characterization of the rovibronic coherence is possible through time-gated frequency-resolved CARS measurements, as recently described.[23] In the matrix, the elimination of rotations renders iodine into a one-dimensional oscillator in a bath. As such, the wave packet framework provides a rather complete and intuitive picture for the description of the process.[24,25] We establish this picture prior to presenting the experimental data and their analysis.

In time resolved four-wave mixing spectroscopies, the third-order polarization. $P^{(3)}$, in response to the application of three short laser pulses is investigated.[26,27] In CARS, commonly, two of the pulses are chosen to have the same color and are identified as pump, P and P'; while the third pulse is identified as Stokes, S, because of its redshift relative to the pump. The component of the polarization propagating along the anti-Stokes wave vector, $\mathbf{k}_{AS}=\mathbf{k}_p+\mathbf{k}_{p'}-\mathbf{k}_S$, is then spatially filtered and monitored as a signal. It is the bulk polarization that defines the wave vectors. In the long-wave limit, and under resonant conditions, it is sufficient to consider the molecular polarization. Moreover, by choosing pump and Stokes colors to overlap with the dipole allowed $X(^1\Sigma_{0_g^+})\leftrightarrow B(^3\Pi_{0_u^-})$ transition of iodine, the consideration may be limited to strictly resonant scattering over the two

a)Electronic mail: aapkaria@uci.edu

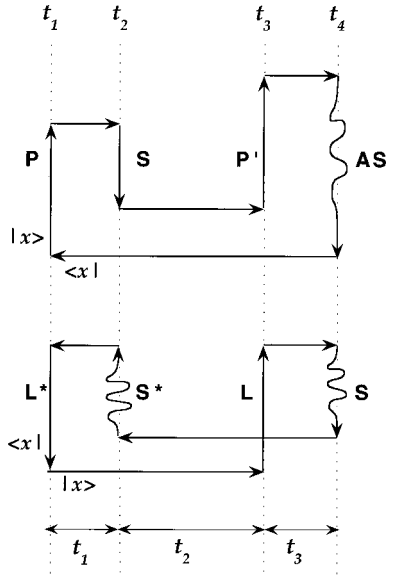

FIG. 1. Time circuit diagrams. (Top) The experimentally selected CARS process, with times indicating interaction with field; (bottom) resonant Raman scattering (only R_3 component) (Ref. 27) with times indicating intervals between interactions. The horizontal lines imply propagation—on the ground electronic state (lower line) or excited electronic state (upper line). Arrows indicate the sense of time. Both processes are given by three-time correlation functions. In the case of RR, the two-wave process is represented by the four interactions due to complex conjugation (*): L indicates laser radiation at ω_L, S indicates scattered radiation at ω_S.

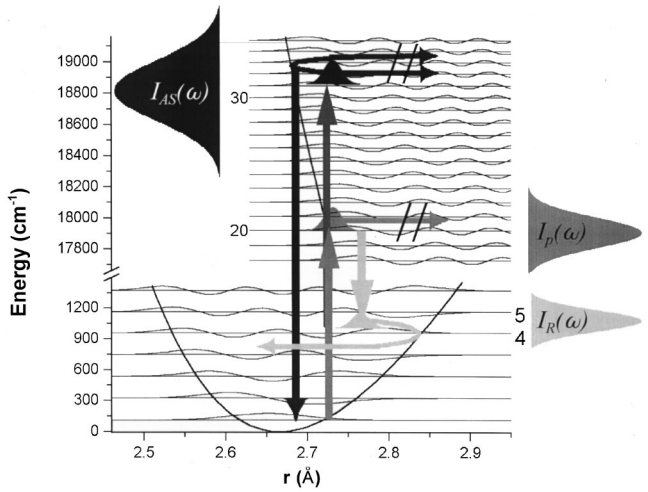

FIG. 2. Wave packet picture for electronically resonant CARS in iodine. The spectral intensity distributions of pump laser, $I_P(\omega)$, the Raman window, $I_R(\omega)=I_P(\omega)*I_S(\omega)$ and the anti-Stokes polarization, $I_{\mathrm{AS}}(\omega)$, correspond to those used in the measurement of the two-state superposition. The thickness of the arrows are made to approximate the P, S, and P' windows along the molecular axis. The coherence decays due to wave packet motion on the excited state, as the molecule stretches. This guarantees that the AS radiation only occurs during bond compression—only the negative component of the Raman packet evolving on the ground electronic state can contribute to the CARS signal.

electronic state Hamiltonian, $H=|X\rangle H_X\langle X|+|B\rangle(H_B+T_e)\times\langle B|$, and the rotating wave approximation becomes valid. For the experimentally selected sequence of pulses, P followed by S followed by P', the AS radiation is given in third-order time-dependent perturbation,

$$P^{(3)}_{\mathbf{k}_{\mathrm{AS}}}(t)=\frac{k}{\hbar^3}\int_{-\infty}^{t}dt_3\int_{-\infty}^{t_3}dt_2\int_{-\infty}^{t_2}dt_1 e^{-i(\omega_P-\omega_S+\omega_P)t}\times\langle\varphi_X e^{iH_X t/\hbar}|\hat{\mu}|e^{-iH_B(t-t_3)/\hbar}\hat{\mu}E_P(t_3)\times e^{-iH_X(t_3-t_2)/\hbar}\hat{\mu}E_S^*(t_2)\times e^{-iH_B(t_2-t_1)t/\hbar}\hat{\mu}E_P(t_1)e^{-iH_X t_1/\hbar}\sigma_X\rangle+\mathrm{c.c.}, \tag{1}$$

in which H_B and H_X are the vibrational Hamiltonians in the excited and ground electronic states, respectively: $E_1(t)$ is the pulse envelope associated with the field at carrier frequency ω_1, and $\hat{\mu}=\mu(|\varphi_X\rangle\langle\varphi_B|+|\varphi_B\rangle\langle\varphi_X|)$ is the dipole operator. For a nonoverlapping sequence of pulses, the single time ordering of interactions explicit in (1) applies. This can be represented diagrammatically using the Feynman-type time circuit diagram of Fig. 1(a).[4,6] Since in a cryogenic matrix the initial population is limited to $X(v=0)$, the choice of ω_p near the absorption maximum and $\omega_p-\omega_s \gg k_BT$ ensures that the S pulse is ineffective in promoting amplitude via the $B\leftarrow X$ transition. This ensures that the single diagram remains operative even when P and S pulses coincide.

The content of Eq. (1) can be readily visualized in the wave packet picture illustrated in Fig. 2. For all times, the bra state vector $\langle\varphi_X^{(0)}(t)|$ evolves subject to the ground state Hamiltonian. The fields act on the ket state. At t_1, the pump prepares a wavepacket in the B-state, $|\varphi_B^{(1)}(t)\rangle$, in the Franck–Condon window carved out by the pump laser. In this first-order coherence, the packet on the B potential evolves until $t=t_2$, when the Stokes pulse arrives. The portion of the packet that overlaps with the Stokes window can now be transferred to prepare the second-order (or the Raman) packet, $|\varphi_X^{(2)}(t)\rangle$. The Raman packet evolves on the X state until $t=t_3$, when the P' pulse acts. Now, amplitude proportional to the overlap of the Raman packet with the pump window is transferred to the B-state, to prepare the third-order packet $|\varphi_B^{(3)}(t)\rangle$. In this third-order coherence, the requirement of energy conservation $\delta[\omega_{\mathrm{AS}}-(2\omega_P-\omega_S)]$ for AS radiation can only be met when the packet reaches the inner turning point of the B-potential. This defines the AS window along the $I-I$ coordinate (see Fig. 2).

The condition of coherence is given by the requirement that the dipole-projected ket-state be in phase with the initial bra-state (which evolves field free). With the help of the time-circuit diagram of Fig. 1(a), this condition is specified as

$$\Omega=(E^X_{v=0}(t_4-t_1)-E^B_{v'}(t_2-t_1)-E^X_{v''}(t_3-t_2)-E^B_{v'''}(t_4-t_3))/\hbar=2\pi n. \tag{2}$$

We will identify the initial state indices without primes, while indices in first-, second-, and third-order coherences are identified by one, two, and three primes, respectively. In the absence of sources of decoherence, such as scattering of phonons from the chromophore, the AS radiation persists.[23] It terminates with the decay of the third-order coherence. The requirement of phase coherence in CARS is contained in (2).[28] Loss of phase memory during evolution in any one of

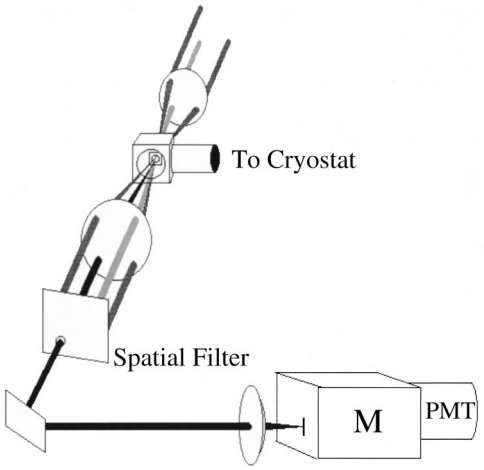

FIG. 3. Experimental setup. The forward BOXCARS configuration is used. A pinhole serves as spatial filter, a 1/4-m monochromator (M) and interference filter are used for spectral filtering of the AS signal.

the coherences leads to decay of the signal. During the intervals t_2-t_1 and t_4-t_3, the system is in an electronic coherence, and therefore subject to electronic dephasing, while during t_3-t_2 the system is a vibrational coherence on the X state (an electronic population on X) therefore subject to vibrational dephasing on the ground electronic state. Incoherent, statistical populations do not contribute to CARS.

To be clear about the similarity of information content in frequency domain RR spectra and in TRCARS, in Fig. 1(b) we provide the time circuit diagram for RR scattering [only the $R_3(t_2-t_1,t_3-t_2,t_4-t_3)$, component of the RR response is shown].[27] Both processes involve propagation on the ground electronic state at intermediate time, t_3-t_2, sandwiched between short propagations on the excited state at t_2-t_1 and t_4-t_3. Although RR is a two-wave process while CARS is a four-wave process, the signal in both cases is given by three-time correlation functions (the three time intervals between four interactions with the radiation field).[27] Explicit atomistic descriptions of the RR scattering process in many-body systems has recently been obtained through the semiclassical evaluation of the three-time correlation function using forward–backward propagation,[29,30] as suggested by the time-circuit diagrams, see Ref. 4. The present experiment allows direct verification of the theoretical description derived from the semiclassical model.

II. EXPERIMENT

The measurements are implemented in the forward BOXCARS geometry, descriptive of the corners of the box made by the four beams,[31] see Fig. 3. Three fs pulses, in two colors, propagating along separate wave vectors are used. The laser system consists of an Ar^+-ion pumped Ti:Sapphire oscillator, the output of which is chirped-pulse amplified at 1 kHz, to 700 μJ/pulse, and compressed to 70 fs. The pulse is split with a 50% beam splitter, to pump two three-stage optical parametric amplifiers (OPA). The OPA output is frequency up-converted by sum generation, to provide tunability in the 480–2000 nm spectral range. The pulse duration and spectrum of each OPA is separately optimized with two-prism compressors. The two pump pulses are obtained by splitting the output of one of the OPAs. The second OPA generates the Stokes pulse. After passing through separate delay lines, the three horizontally polarized beams are focused onto the matrix through a 25-cm achromatic doublet. A pinhole placed immediately behind the cryostat serves as spatial filter. Spatial filtering alone is not sufficient to eliminate scattered laser light. Spectral filtering of the AS beam is necessary to reject scattered light from matrix and substrate. This is achieved with an interference filter centered on the AS wavelength with a 12 nm bandpass, followed by a 1/4-m monochromator adjusted to accept the full filter bandpass. Note, the AS spectral distribution given by the triple convolution of pulses, $I_{\mathrm{AS}}(\omega)=I_P(\omega)*I_S(\omega)*I_P(\omega)$, is rather broad. It can be obtained experimentally as the nonresonant CARS spectrum by inserting a thin glass plate at the focal plane of the beams with all three pulses in space–time overlap. The experimentally determined AS spectral distribution, pump laser spectrum, and the Raman spectral distribution, $I_R(\omega)=I_P(\omega)*I_S(\omega)$, used in one of the measurements are illustrated in Fig. 2. The time and frequency integrated AS beam is detected using a photomultiplier and boxcar integrator. Typically, 100 pulses are averaged for every time delay. To reduce sample degradation, the data are collected at an irradiation rate of 125 Hz, and the laser energy is reduced using a neutral density filter to less than 100 nJ per pulse.

The key to the success of the experiments is the preparation of nonscattering films. This is required to establish spatial coherence to define the polarization wave vectors, and to provide the spatial filtering crucial for reaching a zero-background signal on which the sensitivity of the method rests. The films are prepared by depositing a premixed gas sample of I_2/Ar at a mole fraction of 1:5000, using a pulsed valve (General Valves) operating at 0.5 Hz, with a pulse width of 30 ms, and at a backing pressure of 200–500 Torr. The matrix is deposited on a thin sapphire substrate maintained at 31 K throughout the experiment. The resulting films, of estimated thickness 100 μm, are transparent to the eye, with a faint pinkish hue. The experiments are carried out at the deposition temperature of 31 ± 1 K. Variation of temperature outside this range leads to cracking of the films, increased optical scattering, and severe degradation of the CARS signal.

III. RESULTS

The data are acquired with pump and Stokes pulses nominally in coincidence (in practice, a small relative delay is introduced while optimizing the signal), as a function of delay of the P' pulse. Negative time, $t_<$, corresponds to the P' pulse preceding the $P+S$ pair. In this case, the signal probes the excited state dynamics as it evolves over the t_2-t_1 time interval in the first-order coherence,

$$S(t_<)=\int_{-\infty}^{\infty}dt_4\{P^{(3)}_{\mathbf{k}_{\mathrm{AS}}}(t_4:\delta[t_3-t_2],t_2-t_1)\}^2. \tag{3}$$

At positive time, $t_>$, the coincident $P+S$ pair prepare the

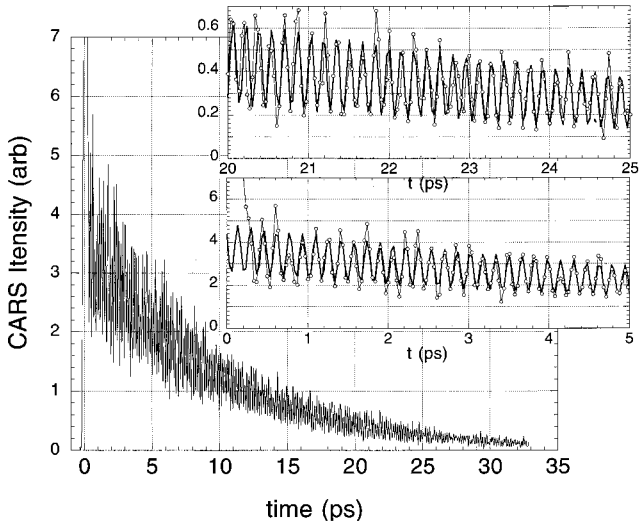

FIG. 4. TRCARS signal for a Raman packet consisting of a two-state superposition. In the expansions, the connected open circles are the experimental points and the solid line is the fit to Eq. (5) of text. A single frequency component (see Table I) reproduces the oscillation periods for the full length of the scan. The noise is mostly in amplitude fluctuations. The spectral composition of the lasers used in this measurement is illustrated in Fig. 2.

Raman packet on the ground electronic state; and the delayed P' pulse probes evolution of this second-order coherence over the t_3-t_2 interval,

$$S(t_>)=\int_{-\infty}^{\infty} dt_4\{P^{(3)}_{\mathbf{k}_{AS}}(t_4:t_3-t_2,\delta[t_2-t_1])\}^2. \tag{4}$$

In Fig. 4 we show the signal obtained with lasers centered at $\omega_P=17\,800\ \mathrm{cm}^{-1}$ (FWHM=194 cm^{-1}), and $\omega_S=16\,827$ (FWHM=212 cm^{-1}). It consists of a saturated peak at the time origin, the noise floor at negative time, and a deeply modulated signal that can be followed for ~30 ps at positive time. At $t=0$, when all three pulses coincide, nonresonant scattering from the matrix and substrate contribute to produce the saturated signal. The absence of a signal at negative times, outside the $t=0$ peak, implies that the first-order coherence does not contribute signal outside the coincidence of pulses. We may conclude that evolution of the $\varphi^{(1)}_B(t)$ packet on the *B*-state leads to decay of the signal prior to any recursions. The same must hold for the third order coherence, $\varphi^{(3)}_B(t)$, since it too involves wave packet evolution on the excited *B*-state. This has the interesting consequence of momentum filtering, to which we will return below. At positive time, when the Raman packet $\varphi^{(2)}_X(t)$ is probed, the oscillatory signal decays with a halflife of 10 ps, and ~200 distinct oscillations can be seen within the dynamic range of the measurement. Evidently, evolution of the Raman packet on the ground electronic state occurs with retention of phase coherence for ~10 ps.

The experimental waveform at positive time can be decomposed as a sum of damped sinusoids,

$$S(t_<)=\sum_{i=0}^{n} A_i\cos(\omega_i t+\phi_i)e^{-t/\tau_i}. \tag{5}$$

TABLE I. Decomposition of waveforms according to Eq. (5).

Two-state superposition				
i	A_1	τ_1	$\omega_1\,(\mathrm{cm}^{-1})$	$v'-v$[a]
0	1	10 ± 1	0	⋯
1	0.37	9.8 ± 0.6	207.35±0.03 (208.44)[b]	4–3

Three-state superposition					
i	A_1	τ_1	ϕ_1	$\omega_1\,(\mathrm{cm}^{-1})$	$v'-v$
0	1	10±1	⋯	0	⋯
1	0.3	9.5±2	55°	207.35±0.03 (208.44)	4–3
2	0.45	11±1	0°	208.49±0.03 (209.67)	5–4
3	0.1	9±2	210°	415.9±0.15 (418.11)	5–3

[a]Vibrational assignment.
[b]Based on gas phase parameters, $\omega_e=214.57$, $\omega_e x_e=0.6127$.

Estimates of the parameters in (5) are first obtained from the Fourier transform of the waveform, then optimized by a nonlinear least squares fit in time domain. The fit in Fig. 4 contains only two terms—a zero frequency component and one oscillating term. The best-fit parameters are collected in Table I. Note, for a single oscillating term the phase is determined by the time origin, which is not known with sufficient accuracy to yield a meaningful value. We also note that the decay times of the two components are the same within experimental error. The expanded scale comparisons of signal and fit in Fig. 4 are provided to demonstrate that a single frequency reproduces the entire waveform. This frequency is determined with an accuracy of $\pm 0.03\ \mathrm{cm}^{-1}$. We may conclude that a two-state vibrational superposition is being observed, with a beat frequency of $207.35\pm0.03\ \mathrm{cm}^{-1}$ given by the energy spacing between eigenstates. This spacing is closest to the gas phase separation between vibrational states 6 and 5, $G(v=6)-G(v=5)=207.22\,\mathrm{cm}^{-1}$. However, based on the Raman window (see Fig. 2), the more likely assignment of superposition is $v=4$, 5. This assignment will be further supported below. Note, a shift by one quantum number can occur if the harmonic frequency of $I_2(X)$ in solid Ar is reduced by $2\omega_e x_e=1.225\,\mathrm{cm}^{-1}$ from its gas phase value of $\omega_e=214.57$.[32]

The CARS signal shown in Fig. 5 is obtained with nearly unchanged central frequencies, $\omega_P=17\,721\,\mathrm{cm}^{-1}$ and $\omega_S=16\,862\,\mathrm{cm}^{-1}$, but with pump and Stokes bandwidths increased to FWHM=314 cm^{-1} and 426 cm^{-1}, respectively. The spectral convolution of these nontransform limited pulses has a FWHM=530 cm^{-1}, comparable to three vibrational spacings in the *X* state. The signal is detected with a bandpass of 430 cm^{-1}. The absence of recurrences in third-order coherence is most directly established by the absence of structure in the CARS spectral window, and therefore the absence of any dependence of the signal on spectral bandpass.[23] The latter was verified experimentally by tuning the detection bandpass with the tilt angle of the interference filter. Beside the zero-frequency component, the Fourier spectrum of the waveform now consists of two resolved fundamentals, at 208.49 cm^{-1} and 207.35 cm^{-1}, and an overtone, at 416.1 cm^{-1}, (see insets to Fig. 5). The best-fit parameters of the waveform to (5) are collected in Table I. As discussed above, only relative phase shifts $|\phi_1-\phi_1|$ are

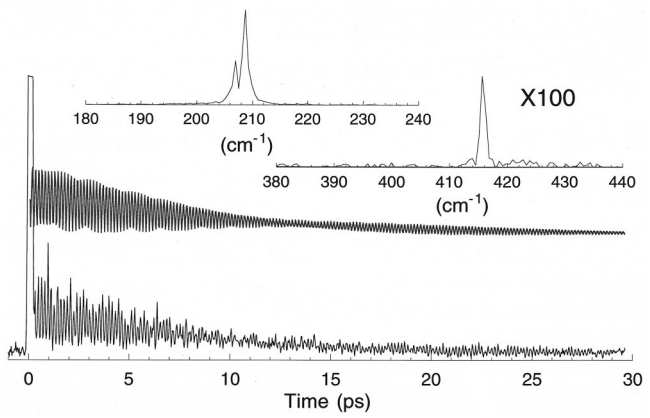

FIG. 5. TRCARS signal for a Raman packet consisting of a three-state superposition. The power spectrum, consisting of two fundamental frequencies and one overtone, identifies the packet as a three-state superposition. The data in this case is obtained with chirped pulses.

meaningful. Again, decay constants of all frequency components are within the experimental error bars. The extracted frequencies are quite precise. The comparison between fit and signal at long time establishes that the noise in the data is mostly in amplitude—the periods of oscillation remain in synchrony with the fit for the ~200 observed cycles. Consistent with the assignment of the two-state superposition, based on the Raman spectral window dictated by the convolution of P and S pulses, the three observed states can be assigned with confidence to $v=3, 4, 5$. The observed fundamentals correspond to the beats $\omega_1=G(5)-G(4)$ and $\omega_2=G(4)-G(3)$, while the overtone corresponds to $\omega_3=G(5)-G(3)$.

Assuming first order anharmonicity, $G_{1/2}(v)=\omega_e(v+1/2)-\omega_e x_e(v+1/2)^2$, two assigned level spacings is sufficient to extract a harmonic frequency, $\omega_e=213.05\pm0.05\ \mathrm{cm}^{-1}$ and an anharmonicity, $\omega_e x_e=0.57\pm0.03\,\mathrm{cm}^{-1}$, to be compared to the gas phase values of 214.57 cm^{-1} and 0.627 cm^{-1}, respectively.[32] Thus in Ar, the harmonic frequency of iodine is reduced by 1.5 cm^{-1} (0.7% relative to the gas phase). This determination is in good agreement with the analysis of RR spectra of I_2 in matrix Ar.[5,6] In the present, the extracted molecular parameters are based on two spacings, while the RR parameters are based on a linear fit to ~15 vibrational spacings from an observed sequence of ~20 overtones. The spectral resolution of ±0.03 cm^{-1} in the present, is determined by the time length over which the beats can be observed. In the RR spectra, the low photon counts and the limited ability of the matrix to dissipate high laser intensities, necessitate the recording of spectra at a resolution of 5–10 cm^{-1}. The accuracy of the parameters extracted from the RR spectra derives from the length of the observed sequence.

By definition, the decay of the CARS signal measures the loss of coherence–decoherence. The decay of the signal over t_3-t_2 interval measures decoherence due to evolution on the ground electronic state, after a short evolution on the excited B state. The same decay time determines RR linewidths. The observed coherence decay time of 10 ps implies a linewidth of 3 cm^{-1}, which is significantly narrower than the instrumental resolution used in the extant RR measurements in matrices. In effect, the present TRCARS measurements are of higher spectral resolution than the existing frequency domain RR measurements.

IV. DISCUSSION

In the observed waveforms, the absence of frequencies other than that of molecular iodine indicates that the Raman packet is a zero-phonon superposition. The only observable effect of the host is the exponential decay of the signal. As such, the experiment is a realization of the idealized one-dimensional Morse oscillator in a bath (with strong coupling in the excited electronic state and weak coupling near the bottom of the ground electronic state). Within this frame, it is useful to consider the dynamics that shape the observed waveform, and in particular, the effect of the absence of recursions in $\varphi_B^{(1)}(t)$, and therefore in $\varphi_B^{(3)}(t)$. Rather than the observed frequencies, which were already analyzed in Sec. III, we are interested in understanding the depth of modulation of the signal in the language of packets and windows used in Sec. I.

First let us note that the strictly temporal interpretation of the signal in terms of quantum beats ignores the evolution of vibrational superpositions under the laser pulses. While appropriate for spins or pure rotations,[33] in the case of vibrations, this interpretation corresponds to the strictly impulsive limit of Eq. (1), in which the various time integrals can be regarded as Fourier filters that select specific components of the third-order polarization. The language of packets and windows can be used, see Appendix A, to obtain the standard result in state representation,

$$S(t)\propto\sum_v c_v^2 e^{-2\Gamma_v t} + 2\sum_{v,v'\neq v} c_v c_{v'}\cos[(\omega_v-\omega_{v'})t]e^{-(\Gamma_v+\Gamma'_{v'})t} \qquad (6)$$

in which the coefficients of eigenstates, c_v, contain vibronic transition matrix elements, and the amplitude decay constants, Γ_v, are introduced phenomenologically. According to Eq. (6) the depth of modulation of the signal depends on the disparity between coefficients of eigenstates. Where $c_v=c_{v'}$ the signal is fully modulated; otherwise, the coherent population terms (square terms) generate the zero-frequency component in the signal. The finite pulse width result is obtained by convolution of the impulse response with the time profile of the laser. The convolution reduces the depth of modulation, in effect increasing the amplitude of the zero-frequency component and reducing the amplitudes of oscillating terms [A_0 and A_1 in Eq. (5)]. Hence the use of the functional form with unrestricted amplitudes, Eq. (5), to fit the data. Decomposition of the signal in terms of state specific decay times, with the constraints on parameters provided by Eq. (6), is possible. Although a slightly improved fit can be obtained by allowing the $1/\Gamma_1$ time constants to differ by 10%, the improvement is marginal. Within experimental error, all eigenstates decay with the same time constant.

The decay constants, Γ_1, introduced in Eq. (6) are for amplitudes of eigenstates. Since a single decay constant characterizes the experimental signal, then $1/\tau=2\Gamma=10\pm1$ ps is identified as a generic decoherence time. Even though the squared term in Eq. (6) has the appearance of vibrational population, the decay rate of the zero-frequency term in Eq. (5), may not be assigned to a T_1-type population decay. The fitting form of Eq. (5), as obvious from the derivation of Eq. (6), does not discriminate between relaxation of vibrational population or dephasing; the latter being the loss of the required phase correlation defined in Eq. (2). Mechanically, both processes involve the exchange of energy between chromophore and bath degrees of freedom. In dephasing, the scattering of thermal phonons on the molecular center generates phase noise—a change of period, $\hbar/\Delta E$, small in comparison to the natural period given by the vibrational spacing, $\hbar/(E_v-E_{v-1})$.[6] While in the case of population relaxation, the scattering leads to irreversible flow of vibrational energy from molecule to bath. Both vibrational dephasing and relaxation rates are expected to be proportional to vibrational quantum numbers,[34,35] yet we do not observe a discernible variation among the three observed states. The experiment does not allow a direct identification of the decay mechanism.

In the absence of the effect of the host, which evidently can be introduced *a posteriori*, we are left with a one-dimensional problem. In 1D, Eq. (1) can be evaluated exactly, by sequential numerical integrations to obtain the various order wave functions, and expected signal. The results of such treatments are already familiar in the literature, in the context of TRCARS studies of iodine vapor.[22] We are interested in aspects of the scattering process that are peculiar to the condensed phase. To this end, consider the Raman packet given by numerically integrating Eq. (1) over t_1 and t_2,

$$\varphi^{(2)}(t)=\sum_v a_v(t)|v_X\rangle e^{-iE_v^X t/\hbar} \tag{7}$$

in which the vibrational eigenfunctions are obtained from the one-dimensional, bare molecular potential, and the time dependent coefficients are evaluated explicitly,

$$\begin{aligned} a_v(t)=&\left(\frac{-i}{\hbar}\right)^2\mu^2\sum_{v'}\langle v|v'\rangle \\ &\times\langle v'|0\rangle\int_{-\infty}^{t}dt_2\int_{-\infty}^{t_2}dt_1E_S(t_2) \\ &\times e^{-i(\omega_S-(E_v-E_{v'})/\hbar)t_2}E_P(t_1) \\ &\times e^{-i(\omega_P-(E_v-E_{v'=0})/\hbar)t_1}. \end{aligned} \tag{8}$$

In the evaluation we assume transform limited Gaussian pulses, $E_L(t)$, with widths determined by the experimental laser spectra. The obtained time evolution of state coefficients, $|a_v(t)|$, in the Raman packet are shown in Fig. 6. The packet consists predominantly of $v=4$ and $v=5$, confirming the assignment made above. Snapshots of $\varphi_B^{(1)}(t)$ and $\varphi_X^{(2)}(t)$ during preparation are shown in Fig. 7. The early time snapshots, at $t<90$ fs, make it clear that the packets are born in a relatively narrow window along the molecular coordinate: FWHM ~0.02 Å for $\varphi^2(x)$. This is a result of the steep repulsive wall of the excited state and justifies the use of classical probe windows in analysis. Mapping of the windows on the eigenfunctions, as widths of arrows in Fig. 2 makes it clear that due to the very narrow transition windows, Franck–Condon factors that control state participation can be quite irregular. Then, by systematically scanning carrier frequencies of *P* and *S* pulses, *it should be possible to map out X-state wave functions.*

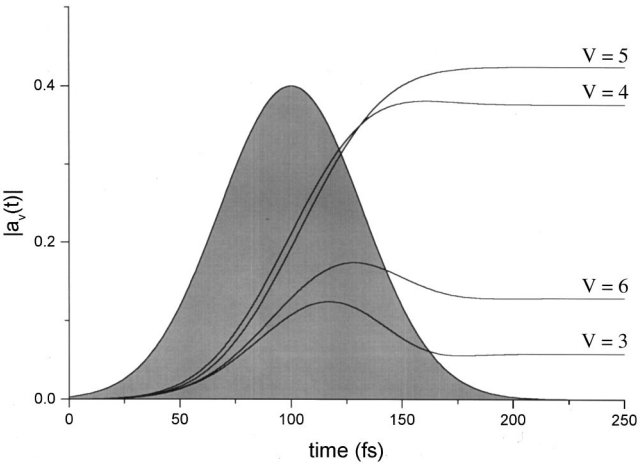

FIG. 6. Time dependence of state coefficients in the Raman packet. The shaded Gaussian is the intensity envelope of the pump pulse, the Stokes pulse is assumed coincident and has nearly identical pulse width. The signal is proportional to the squares of the coefficients. The packet is a two-state superposition consisting of $v=4$, 5 on the *X* state.

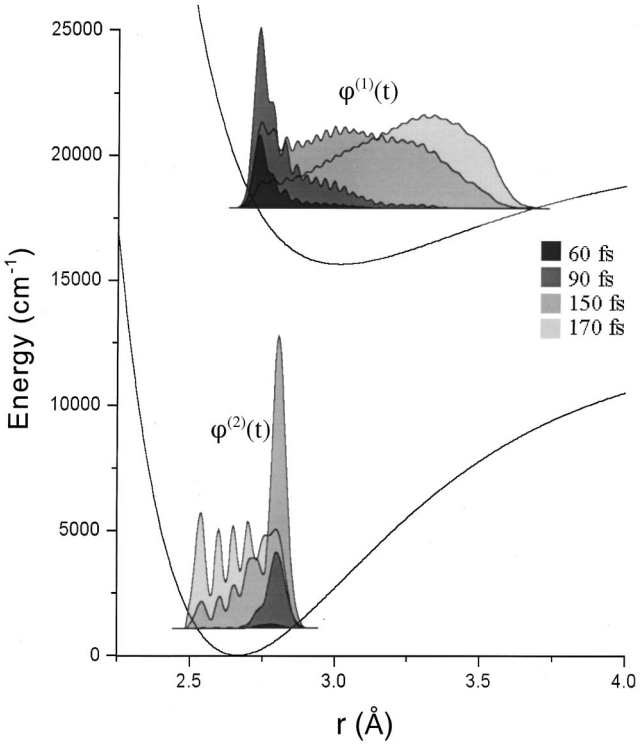

FIG. 7. Snapshots of the first and second order packets evolving under the coincident $P+S$ pulses. The peak of the laser pulse occurs at $t=100$ fs, as in Fig. 6.

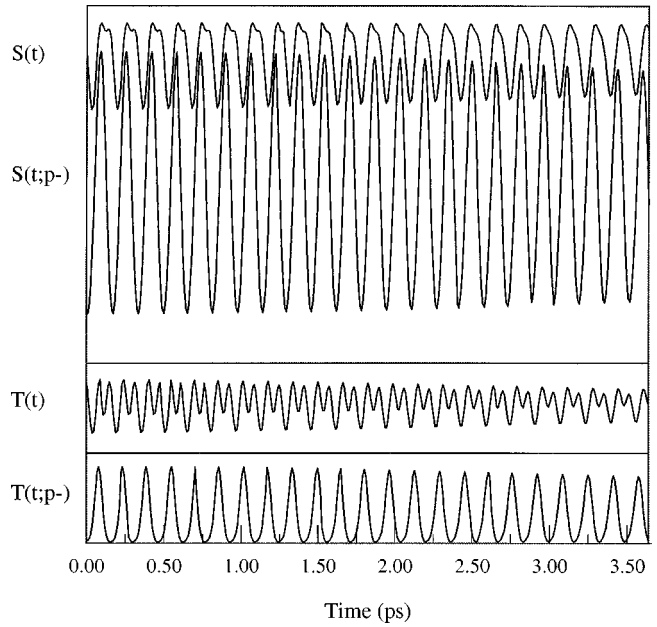

FIG. 8. The effect of momentum filtering. The transfer function. $T(t)$, is defined as the impulse response [Eq. (10) of text], and the signal is defined as the finite pulse width response obtained by Gaussian time convolution [Eq. (11) of text]. In the absence of filtering, the signal shows a doubling of the periodic resonance, which in turn leads to a shallow depth of modulation. The momentum filtered Raman packet [Eq. (12) of text] yields $T(t;p-)$, in which the doubling is eliminated, and accordingly, a deeply modulated signal, $S(t;p-)$, is obtained.

The visibility of a given eigenstate, namely its contribution to the observed signal, is subject to filtering by the P' pulse. The signal can be regarded as the overlap of the Raman packet with the time-dependent second-order window, $W^{(2)}(t)$, obtained in state representation by proceeding from the left-hand side of Eq. (1) to integrate over t_4 and t_3 (see Appendix). Nearly identical results are obtained by approximating the action of the P' pulse as a time-dependent window which is stationary along the molecular coordinate, by defining the probe window along the molecular axis through the reflection approximation, i.e., assumption of exact conservation of kinetic energy during the vertical transition,

$$W^{(2)}(q)=\int_{-\infty}^{+\infty} dt e^{-i\omega_P t} e^{i(T+V)_B t/\hbar} \mu E_{P'}(t) e^{-i(T+V)_X t/\hbar}$$
$$=\mu E_{P'}(\omega)\,\delta[\hbar\omega-(V_B(q)-V_X(q))]. \tag{9}$$

For signal proportional to the overlap of window and packet, the impulse response defines the transfer function,

$$T(t)\propto\langle W^{(2)}(q)\varphi^{(2)}(q,t)\rangle^2. \tag{10}$$

The signal is obtained as the response to a finite P' pulse,

$$S(t_>)=c\int d\tau E_P^2(t-\tau)T(\tau). \tag{11}$$

In Fig. 8 we show the resulting transfer function, $T(t)$, and the signal, $S(t_>)$. The transfer function clearly shows the splitting of the periodic resonance (period doubling), due to the separation in time of the positive and negative momentum components of the wavepacket as they enter the P' window. A symmetric period doubling is obtained when the probe window is located in the middle of the molecular bond. The convolution (11) eliminates the doubling, but at the price of dramatically reducing the depth of modulation of the signal to $\approx$25% [see $S(t)$ in the top panel of Fig. 8]. This clearly does not agree with the experiment, see Fig. 4. The assumption in Eq. (10) is that the entire amplitude promoted by the P' pulse contributes to the AS polarization. Since the first order coherence decays prior to recursion, we may be sure that *the positive momentum component of* $\varphi_B^{(3)}(t)$ *prepared by the* P' *pulse will dephase before it can reach the AS window, and therefore cannot contribute to the signal*. Only the negative momentum component of $\varphi_B^{(3)}(t)$ may contribute to the signal. The vertical nature of the optical transition, in turn, implies that only the negative momentum component of $\varphi_X^{(2)}(t)$ may contribute to the signal.[36] Accordingly, we filter out the negative momentum component of the Raman packet, by transforming it to momentum space, eliminating the positive momentum component by multiplication with the unit step function $H_<(0)$, and back transforming to coordinate space,

$$\varphi_X^{(2)}(t;p-)=\int_{-\infty}^{\infty} dp e^{ipq/\hbar} H_<(0)\int_{-\infty}^{\infty} dq e^{-ipq/\hbar}\varphi_X^{(2)}(t), \tag{12}$$

where

$$H_<(0)=\begin{cases}0 & \text{for } p>0\\ 1 & \text{for } p<0\end{cases}. \tag{13}$$

The filtered Raman packet is then used in Eq. (10) to simulate the signal. The resulting transfer, $T(t,p-)$, and signal, $S(t;p-)$, functions are shown in Fig. 8. A direct comparison is made with the experiment in Fig. 9, after multiplying the simulated signal with a 10 ps exponential decay. The filtering eliminates the period doubling in the transfer function (Fig. 8), and the depth of modulation of the simulated waveform is in excellent agreement with the experiment (Fig. 9). It is necessary to take the effect of momentum filtering into account to reproduce the CARS signal of I_2 in solid Ar. Moreover, it has been verified that under similar excitation conditions a significantly shallower depth of modulation is attained in the gas phase.[37]

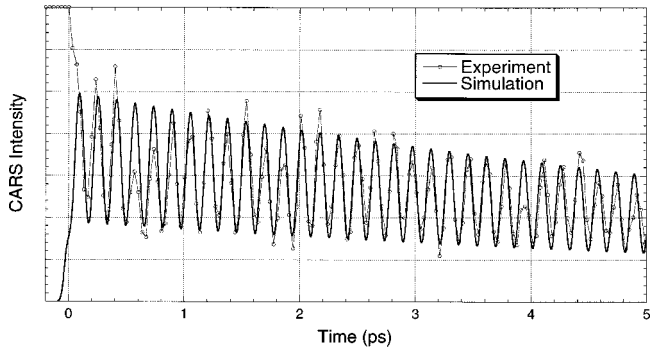

FIG. 9. Comparison between simulated momentum-filtered signal and experiment. For the comparison, an exponential decay of 10 ps is included in the simulated signal.

V. CONCLUSIONS

We have been able to grow matrix films of I_2 doped Ar of sufficiently high optical quality to enable nonlinear optical measurements, in this case, time resolved CARS. The absence of recurrences in first order coherence, during evolution on the excited state, and the lack of structure in the CARS spectrum, establish that in the condensed phase, the first- and third-order coherences decay prior to recursion. This information was already available in the absorption spectra of iodine, in the fact that the spectra are not structured.[38] Note, while pump–probe measurements have been used to monitor vibrational coherences on the excited B state,[39] CARS cannot yield the same information due to the fast electronic dephasing in the process.[28] In contrast, the Raman prepared packets near $v=4$ of the ground electronic state can be followed for some 200 recursions using CARS. This information was qualitatively known by the fact that RR spectra show a relatively sharp progression of lines.[40] The present experiments establish that the decoherence time on the ground electronic state, in the solid, is 10 ps; while from instrument limited linewidths of RR spectra it had been estimated that the coherence decays on a time scale of ~ 3 ps.[6] The long-lived Raman packet allows rather accurate evaluations of frequencies and anharmonicities in the ground electronic state, in effect allowing an accurate description of the solvated molecular potential. Based on the measurement of two vibrational spacings, we have extracted ω_e and $\omega_e x_e$ values for the bottom of the potential, a more extensive measurement would clearly be valuable.

We have argued and demonstrated that the CARS signal is subject to a momentum filter as a necessary outcome of the absence of recursions in $\varphi_B^{(1)}(t)$. We may then state more generally that whenever the absorption spectrum is structureless, the observation of resonant CARS necessarily implies that momentum filtering is in effect. It can therefore be appreciated that the phenomenon is ubiquitous in condensed phase measurements. This leads to the none too obvious conclusion that time resolved resonant CARS spectra of molecules in condensed media can be expected to yield a more deeply modulated signal than in the gas phase. In effect, a higher time resolution is obtained in the condensed phase by elimination of period doubling that occurs whenever the system is probed near the middle of the bond.

It has been previously demonstrated that vibrational coherences can be controlled with chirped pulses on excited electronic states of matrix isolated iodine.[41–43] The fact that Raman prepared packets on the ground electronic state are long lived implies the feasibility of control of vibrational packets on the ground electronic state. Time-resolved CARS gives great flexibility to manipulate packets and to observe them.[44] As an example, it should be possible to launch a packet on the ground electronic state, and to bring it up to the excited state at a configuration where electronic curves cross. This would allow the direct scrutiny of nonadiabatic dynamics in the condensed phase, which remains the guiding motive for developing the described TRCARS experiments.

ACKNOWLEDGMENT

The support of this research through a grant from the U.S. AFOSR (F49620-95-1-0213) is gratefully acknowledged.

APPENDIX

Fitting the experimental CARS signal in terms of damped sinusoids ignores the phase space evolution of vibrational packets. Such a treatment is justified empirically in practice, when experimental time resolution is limited, such that the detailed structure of the waveform is not obtained. This strictly temporal interpretation can be obtained under the strictly impulsive limit; namely, by ignoring the evolution of the molecular Hamiltonian under the pulses as seen in Fig. 7 of the text. In this limit, the time integrals simply reduce to the Fourier filtering of various components of the polarization. Thus, the first interaction with the radiation generates a wave packet,

$$\begin{aligned}\varphi^{(1)}(t_2)&=\int_{-\infty}^{t_2} dt_1 e^{-i\omega_P t_1}\sum_{v'} |v'\rangle\langle v'|e^{iH_B t_1/\hbar}\hat{\mu}E_P(t_1)\\ &\quad\times e^{-iH_X t_1/\hbar}|v=0\rangle\\ &=\mu\sum_{v'} |v'\rangle\langle v'|v=0\rangle\\ &\quad\times\int_{-\infty}^{t_2} dt_1 e^{-i[\omega_P-(E^B_{v'}-E^X_v)/\hbar]t_1}E_P(t_1)\\ &=\mu\sum_{v'} |v'\rangle\langle v'|v=0\rangle E_P(\omega_P)\\ &\quad\times\delta[\omega_P-(E^B_{v'}-E^X_v)/\hbar] \qquad \text{(A1)}\end{aligned}$$

consisting of the eigenstates that can be reached with the spectral distribution of the radiation field, weighted by Franck–Condon factors and transition dipoles. The procedure can be repeated in successive orders; and taking advantage of linearity, the finite time response can be obtained from the impulse response by convolution. It is possible to carry out the evaluation in terms of packet and window. Thus, the Raman packet is obtained by the integration over t_2,

$$\varphi^{(2)}(q,t_3-t_2)=\sum_{v''} a_{v''}|v''_X(q)\rangle e^{-iE^X_{v''}(t_3-t_2)/\hbar}e^{-\Gamma^X_{v''}(t_3-t_2)}, \qquad \text{(A2)}$$

where

$$\begin{aligned}a_{v''}=\mu^2\sum_{v'} &\langle v''|v'\rangle\langle v'|v=0\rangle E_P(\omega_P)\,\delta[\omega_P-(E_{v'}\\ &-E_{v=0})/\hbar]E^*_S(\omega_S)\,\delta[\omega_S-(E_{v'}-E_{v''})/\hbar], \qquad \text{(A3)}\end{aligned}$$

and we have introduced the phenomenological state specific amplitude decay constants. $\Gamma_{v'}$. Describing the effect of the host by the single amplitude decay constant is an approximation suggested by the data. Otherwise, the dissipation of vibrational amplitude is due to the sum over all off-diagonal coupling constants, $\Gamma_v=\Sigma_{v'}\gamma_{vv'}$, which need not lead to a

strictly monotonic decay (it can have oscillations).[45] The coefficients a_v are time independent in Eq. (A2) because of the impulse assumption. We may define the second order probe window under the P' impulse, with the same procedure, but now integrating Eq. (1) from the left to obtain

$$W^{(2)}(q,t_3)=\sum_{v''} b_{v''}\langle v''_X(t_3)|q\rangle\langle q|=\sum_{v''} b_{v''}\langle v''_X(q,t_3)|, \tag{A4}$$

where

$$\begin{aligned} b_{v''}=&\mu^2\sum_{v'''}\langle v=0|v'''\rangle\langle v'''|v''\rangle E_{\mathrm{AS}}(\omega_{\mathrm{AS}})\\ &\times\delta[2\omega_P-\omega_S-(E_{v'''}-E_{v=0})/\hbar]E_P(\omega_P)\\ &\times\delta[\omega_P-(E_{v'''}-E_{v''})/\hbar]. \end{aligned} \tag{A5}$$

The observable instantaneous signal is then given as

$$\begin{aligned} S(t)\propto&\left[\int dq\,W_{P'}(q)\varphi^{(2)}(q,t)+\mathrm{c.c.}\right]^2\\ =&\sum_v c_v^2\cos(\omega_v t)^2 e^{-2\Gamma_v t}\\ &+\sum_{v,v'\neq v} c_v c_{v'}\cos[(\omega_v+\omega_{v'})t]e^{-(\Gamma_v+\Gamma_{v'})t}\\ &+\sum_{v,v'\neq v} c_v c_{v'}\cos[(\omega_v-\omega_{v'})t]e^{-(\Gamma_v-\Gamma_v)t}, \end{aligned} \tag{A6}$$

where $c_v\equiv a_v b_v$ and $t\equiv t_3-t_2$.

Convolution of Eq. (A6) with the laser pulse envelope yields the experimental signal. Since typically the pulses used contain many cycles at the carrier frequency, only the beat at the difference frequency is resolvable. The first two terms will only contribute by their cycle averages,

$$\begin{aligned} S(t)\propto&\sum_v c_v^2 e^{-2\Gamma_v t}+0+2\sum_{v,v'\neq v} c_v c_{v'}\\ &\times\cos[(\omega_v-\omega_{v'})t]e^{-(\Gamma_v-\Gamma_{v'})t} \end{aligned} \tag{A7}$$

which is the result sought, and the basis of the analysis of the experimental waveforms in terms of decaying sinusoids.

[1] R. Zadoyan, J. Almy, and V. A. Apkarian, J. Chem. Soc., Faraday Discuss. **108**, 255 (1997), and references therein.
[2] M. Bargheer, P. Dietrich, K. Donovang, and N. Schwentner, J. Chem. Phys. **111**, 8556 (1999).
[3] N. Bloembergen, Pure Appl. Chem. **10**, 1229 (1987).
[4] For a detailed discussion, see M. Ovchinnikov, V. A. Apkarian, and G. A. Voth, J. Chem. Phys. (submitted).
[5] W. F. Howard and L. Andrews, J. Raman Spectrosc. **2**, 442 (1974); J. Grzybowski and L. Andrews, *ibid.* **4**, 99 (1975); L. Andrews, Appl. Spectrosc. Rev. **11**, 125 (1976).
[6] J. Almy, K. Kizer, R. Zadoyan, and V. A. Apkarian, J. Phys. Chem. **104**, 3508 (2000).
[7] R. J. Gordon and S. A. Rice, Annu. Rev. Phys. Chem. **48**, 601 (1997).
[8] C. S. Guiang, and R. E. Wyatt, J. Chem. Phys. **112**, 3580 (2000).
[9] Y. C. Chen and J. A. Cina, J. Chem. Phys. **110**, 9793 (1999); E. M. Hiller and J. A. Cina, *ibid.* **105**, 3419 (1996); T. J. Smith and J. A. Cina, *ibid.* **104**, 1272 (1996); L. W. Ungar and J. A. Cina, J. Lumin. **63**, 345 (1995).
[10] J. S. Cao, C. J. Bardeen, and K. R. Wilson, J. Chem. Phys. **113**, 1898 (2000); C. J. Bardeen, J. S. Cao, F. L. H. Brown, and K. R. Wilson, Chem. Phys. Lett. **302**, 405 (1999); J. S. Cao, M. Messina, and K. R. Wilson, J. Chem. Phys. **106**, 5239 (1997).
[11] V. A. Ermoshin, A. K. Kazansky, and V. Engel, J. Chem. Phys. **111**, 7807 (1999); H. Dietz and V. Engel, *ibid.* **110**, 3335 (1999).
[12] C. Meier and D. J. Tannor, J. Chem. Phys. **111**, 3365 (1999).
[13] R. Karmacharya, P. Gross, and S. D. Schwartz, J. Chem. Phys. **111**, 6864 (1999).
[14] J. J. Valentini, in *Spectrometric Techniques* (Academic, New York, 1985), Vol. 4.
[15] S. Maeda, T. Kamisuki, and Y. Adachi, in *Advances in Nonlinear Spectroscopy*, edited by R. J. H. Clark and R. E. Hester (Wiley, New York, 1988), p. 253; J. Nibler, *ibid.*, p. 1.
[16] F. Lineberger, R. Stocl, B. P. Asthana, and A. Laubereau, J. Phys. Chem. A **103**, 5655 (1999).
[17] H. Okamoto, H. Hayashi, K. Yoshihara, and M. Tasumi, Chem. Phys. Lett. **182**, 96 (1991).
[18] W. E. Bron, J. Kuhl, and B. K. Rhee, Phys. Rev. B **34**, 6961 (1986).
[19] F. Geist, H. Pascher, N. Frank, G. Bauer, and M. Kriechbaum, Superlattices Microstruct. **12**, 477 (1992).
[20] A. Vierheilig, T. Chen, P. Waltner, W. Kiefer, M. Materny, and A. H. Zewail, Chem. Phys. Lett. **312**, 349 (1999).
[21] A. Zumbusch, G. R. Holton, and X. S. Xie, Phys. Rev. Lett. **82**, 4142 (1999).
[22] M. Schmitt, G. Knopp, A. Materny, and W. Kiefer, Chem. Phys. Lett. **280**, 339 (1997); **270**, 9 (1997); J. Phys. Chem. A **102**, 4059 (1998); T. Siebert, M. Schmitt, A. Vierheilig, G. Flachenecker, V. Engel, A. Materny, and W. Kiefer, J. Raman Spectrosc. **31**, 25 (2000); S. Meyer and V. Engel, *ibid.* **31**, 33 (2000).
[23] R. Zadoyan and V. A. Apkarian, Chem. Phys. Lett. **326**, 1 (2000).
[24] D. J. Tannor, S. A. Rice, and P. Weber, J. Chem. Phys. **83**, 6158 (1985).
[25] W. Domcke and G. Stock, Adv. Chem. Phys. **100**, 1 (1997).
[26] Y. R. Shen, *The Principles of Nonlinear Optics* (Wiley, New York, 1984).
[27] S. Mukamel, *Principles of Nonlinear Spectroscopy* (Oxford University Press, New York, 1999).
[28] Equation (2) allows the traditional distinction between vibrational and electronic contributions of phase coherence, or equivalently, allows to distinguish vibrational and electronic dephasing terms in CARS. To see this, note that $E^B_{v'}=E_{v'}+T_e$, with v' representing all vibrational modes of the guest/host supersystem, while T_e is the electronic origin of the guest molecule. Phase evolution around the time-circuit can be separated into components, $\Omega=[E_{v=0}(t_4-t_1)-E_{v'}(t_2-t_1)-E_{v''}(t_3-t_2)-E_{v'''}(t_4-t_3)]/\hbar-[T_e(t_2-t_1)+T_e(t_4-t_3)]/\hbar$. If we now identify v' by the single vibrational degree of freedom of the chromophore, then all the bath degrees of freedom are contained in the electronic origin, T_e, they lead to modulation of the many-body electronic origin, along with electronic dephasing.
[29] N. Makri and K. Thompson, Chem. Phys. Lett. **291**, 101 (1998); O. Kuhn and N. Makri, J. Phys. Chem. A **103**, 9487 (1999).
[30] X. Sun and W. H. Miller, J. Chem. Phys. **110**, 6635 (1999).
[31] S. Maeda, T. Kamisuki, and Y. Adachi, Adv. Nonlinear Spectrosc. **30**, 807 (1999).
[32] G. Herzberg, in *Spectra of Diatomic Molecules* (Van Nostrand Reinhold, New York, 1950).
[33] T. Lang, K. L. Kompa, and M. Motzkus, Chem. Phys. Lett. **310**, 65 (1999).
[34] H. Eyring, S. H. Lin, and S. M. Lin, *Basic Chemical Kinetics* (Wiley–Interscience, New York, 1980).
[35] G. J. Hoffman, D. G. Imre, R. Zadoyan, N. Schwentner, and V. A. Apkarian, J. Chem. Phys. **98**, 9233 (1993).
[36] A right-traveling packet on the X state cannot yield CARS signal. This is because, a right-traveling packet on the X state when projected to the B state will continue to travel right. According to energy conservation, to radiate an AS photon, it must return to the inner turning point of the B potential. However, the system will dephase prior to a period of evolution on the B state, therefore there will be no coherent radiation. A left going packet when promoted to the B state, will radiate at the left turning point, then turn around to stretch on the B state and dephase.
[37] R. Zadoyan, D. Kohen, and V. A. Apkarian, Chem. Phys. (in press).
[38] M. Ovchinnikov and V. A. Apkarian, J. Chem. Phys. **105**, 10312 (1996).
[39] R. Zadoyan, M. Sterling, and V. A. Apkarian, J. Chem. Soc., Faraday Trans. **92**, 1821 (1996).
[40] M. Ovchinnikov and V. A. Apkarian, J. Chem. Phys. **106**, 5775 (1997).

[41] J. W. Che, M. Messina, K. R. Wilson, V. A. Apkarian, Z. Li, C. C. Martens, R. Zadoyan, and Y. J. Yan, J. Phys. Chem. **100**, 7873 (1996); C. J. Bardeen, J. Che, K. R. Wilson, V. V. Yakovlev, V. A. Apkarian, C. C. Martens, R. Zadoyan, B. Kohler, and M. Messina, J. Chem. Phys. **106**, 8486 (1997).
[42] M. Sterling, R. Zadoyan, and V. A. Apkarian, J. Chem. Phys. **104**, 6497 (1996).
[43] R. Zadoyan, N. Schwentner, and V. A. Apkarian, Chem. Phys. **233**, 353 (1998).
[44] For an example of wave packet manipulation using TRCARS in the gas phase, see G. Knopp, I. Pinkas, and Y. Prior, J. Raman Spectrosc. **31**, 51 (2000).
[45] D. Kohen, C. C. Marston, and D. J. Tannor, J. Chem. Phys. **107**, 5236 (1997).